Morphology Control in Block Copolymer/Polymer Derived Ceramic Precursor Nanocomposites

Marleen Kamperman, Melissa A. Fierke,† Carlos B. W. Garcia,‡ and Ulrich Wiesner*

Department of Materials Science and Engineering, Cornell University, Ithaca, New York 14853

Received June 30, 2008; Revised Manuscript Received September 10, 2008

ABSTRACT: Block copolymer−polymer derived ceramic (PDC) precursor nanocomposites were prepared using amorphous poly(isoprene-*block*-(dimethylamino)ethyl methacrylate) (PI-*b*-PDMAEMA) and semicrystalline poly(isoprene-*block*-ethylene oxide) (PI-*b*-PEO) block copolymers as structure directing agents for poly(ureamethylvinyl)silazane (PUMVS). Studies on hybrid morphologies were performed using small-angle X-ray scattering (SAXS) and transmission electron microscopy (TEM). In the amorphous system, the PUMVS preferentially swells the PDMAEMA, and a systematic increase of the PUMVS to PI-*b*-PDMAEMA weight ratio resulted in lamellar, hexagonally packed cylindrical and body-centered cubic packed spherical morphologies. Crystallization of PEO in PI-*b*-PEO/PUMVS hybrids led to crystalline lamellar morphologies over a large range of PUMVS to PI-*b*-PEO weight ratios. The *d*-spacing of the PI-*b*-PEO/PUMVS hybrids increased only slightly upon PUMVS loading, because the strong chain stretching in the PI block is progressively relaxed as the PUMVS swells the PEO. Annealing of the PI-*b*-PEO/PUMVS system at elevated temperatures led to suppression of the PEO crystallization, resulting in order−order phase transitions.

Introduction

A convenient and effective way to construct well-defined polymer−inorganic nanostructured composite materials is to use block copolymers as structure directing agents. The prevalent route to preparing such hybrid materials is using sol−gel chemistry where a solution containing inorganic precursors and the block copolymer coassemble to form a spectrum of mesophases.[1−3] In these systems the final morphology of the composite is not dictated by free energy considerations only, but also depends on the kinetics of gel formation.

Mixing a low molecular weight thermosetting resin with a block copolymer was shown to be a successful method for the preparation of all-organic nanostructured hybrid materials.[4−6] The low molecular weight resin selectively swells one of the blocks. Well-defined mesophases were observed by systematically increasing the resin to block copolymer volume fraction. Self-assembly was induced by solvent evaporation and was independent from polymerization of the resin, thereby avoiding the kinetic limitations of sol−gel approaches. More recently, we showed that this method can be applied to mixtures of an amphiphilic block copolymer with polymer derived ceramic (PDC) precursors, providing a one-pot-type pathway toward mesoporous high-temperature ceramics.[7,8] In the meantime, similar results have been produced with different structure directing agents[9,10] and with inorganic−organic block copolymers,[11−13] and the approach has been extended toward organosilicate thin films.[14]

This paper explores in more detail the underlying factors controlling morphology of block copolymer−PDC precursor derived hybrid materials. To this end, we investigated morphological differences resulting from the use of either a semicrystalline or an amorphous diblock copolymer as structure directing agents. Poly(isoprene-*block*-ethylene oxide) (PI-*b*-PEO) and poly(isoprene-*block*-(dimethylamino)ethyl methacrylate) (PI-*b*-PDMAEMA) were used as semicrystalline and amorphous polymers, respectively, both systems being amphiphilic. The PDC precursor was a poly(ureamethylvinyl)silazane (PUMVS), the structure of which is shown in Figure 1 together with the molecular structures of the block copolymers.

Blending PUMVS with either the semicrystalline or the amorphous block copolymer is expected to lead to preferential swelling of their hydrophilic domains, i.e., PEO or PDMAEMA (see Figure 1), thereby increasing the effective hydrophilic volume fraction. The hybrid material was solidified by cross-linking the PUMVS with a radical initiator. We show below that the PUMVS does not suppress the crystallization of the PEO in the hybrid materials, resulting in crystalline lamellar morphologies over a wide range of compositions. We further demonstrate that this crystallinity can be suppressed upon annealing of the hybrids at elevated temperatures, resulting in

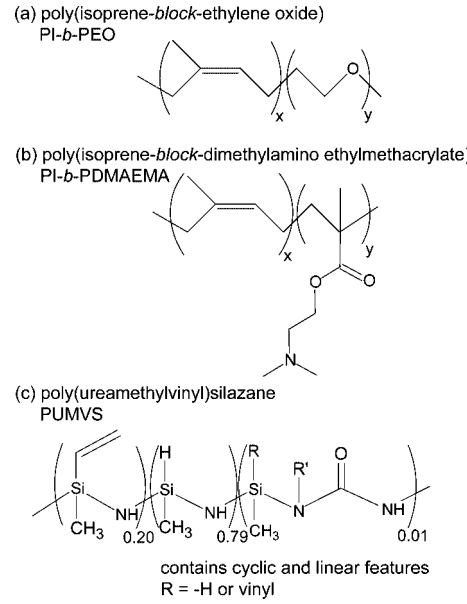

Figure 1. Chemical structures of (a) poly(isoprene-*block*-ethylene oxide), (b) poly(isoprene-*block*-(dimethylamino)ethyl methacrylate), and (c) poly(ureamethylvinyl)silazane (PUMVS). No information is available about the nature of R′.

* To whom correspondence should be addressed. E-mail: ubw1@cornell.edu.
† Present address: Department of Chemistry, University of Minnesota, 207 Pleasant Street SE, Minneapolis, MN 55455.
‡ Present address: Hewlett-Packard IPG R&D, 16399 W Bernardo Dr - MS 61U66, San Diego, CA 92127.

10.1021/ma801458w CCC: $40.75
Published on Web 10/22/2008

a mesophase evolution similar to that in the amorphous block copolymer/PUMVS hybrids, induced by systematically increasing the PUMVS to block copolymer weight fraction. Morphological changes and structural details upon swelling of the hydrophilic block by PUMVS are investigated with small-angle X-ray scattering (SAXS) and transmission electron microscopy (TEM).

Experimental Section

Materials and Instrumentation. *Materials.* For the block copolymer synthesis *sec*-butyllithium (1.4 M in cyclohexane, Aldrich), potassium (98%, Fluka), and naphthalene (99%, Sigma-Aldrich) were used as received. Isoprene (99%, Aldrich), ethylene oxide (99.5+%, Aldrich), cyclohexane (99%, J.T. Baker), tetrahydrofuran (THF) (99%, J.T. Baker), and 1,1-diphenylethylene (97%, Aldrich) were distilled from *n*-butyllithium (1.6 M in hexanes, Sigma-Aldrich) prior to use. The monomer (dimethylamino)ethyl methacrylate (DMAEMA) (98%, Aldrich) was stirred over CaH_2 (90−95%, Aldrich) and distilled under vacuum. Methanolic HCl (3 N, Supelco) was freeze−pump−thawed three times prior to use.

For the hybrid synthesis tetrahydrofuran (99%, J.T. Baker), toluene (99.5+%, J.T. Baker), the ceramic precursor Ceraset (KiON Corp.), and the radical initiator dicumyl peroxide (Aldrich) were used as received.

Instrumentation. Gel Permeation Chromatography (GPC). Measurements were performed in 98% tetrahydrofuran (THF) and 2% *N,N*-dimethylacetamide at room temperature using 5 μm Waters Styragel columns (10^3, 10^4, 10^5, 10^6 Å, 30 cm each; Waters Corp., Milford, MA) at a flow rate of 1.0 mL/min. A Waters 490 programmable multiwavelength UV diode array detector (operated at $\lambda = 260$ nm) and a Waters 410 RI detector operated at 25 °C were used. Raw data were processed using PSS-Win GPC V6.2 software (Polymer Standards Service, Mainz, Germany). Molecular weights (M_w) and M_w distributions (M_w/M_n) were calculated using a polyisoprene calibration curve.

^{1}H Nuclear Magnetic Resonance (NMR). ^{1}H solution NMR spectra were recorded on a Varian INOVA 400 MHz spectrometer using $CDCl_3$ signal ($\delta = 7.27$ ppm) as an internal standard.

Small-Angle X-ray Scattering (SAXS). Experiments were performed at the Cornell High Energy Synchrotron Source (CHESS). Data were collected with a CCD 2-D detector operating at X-ray energy corresponding to 1.223 Å, sample-to-detector distance of 165.0 cm, and exposure times of 1−20 s.

Transmission Electron Microscopy (TEM). Samples were ultrathin sectioned with a Leica Ultracut UCT microtome at −60 °C. Sample slices were collected on a water/DMSO eutectic solution and transferred to 300 mesh copper grids (no carbon film was used). TEM was performed on a Tecnai T12 at 120 kV.

Differential Scanning Calorimetry (DSC). was performed on hybrids with a Thermal Advantage DSC Q100 (TA Instruments, Inc.), calibrated with an indium standard. Before taking measurements, samples were heated to 80 °C, then cooled to −20 °C, and annealed for 1 h at −20 °C. Measurements were taken on heating from −20 to 80 at 5 °C/min.

Synthesis. *Block Copolymer Synthesis.* The general synthetic procedures of the synthesis of poly(isoprene-*block*-ethylene oxide) (PI-*b*-PEO) and poly(isoprene-*block*-(dimethylamino)ethyl methacrylate) (PI-*b*-PDMAEMA) have been previously reported.[15−17] A slightly modified synthesis was used here and is summarized in Scheme 1. Polymers were synthesized by anionic polymerization under anhydrous and air-free conditions using a glovebox and Schlenk line techniques.

PI-b-PEO. sec-Butyllithium was used to initiate isoprene in cyclohexane. After 8 h of polymerization at room temperature, the polyisoprene was end-capped with ethylene oxide and stirred overnight (caution: ethylene oxide is a toxic gas at room temperature!). Polymerization was terminated with methanolic HCl. Cyclohexane was removed by rotary evaporation, and the polymer was washed three times with water in chloroform (50/50 vol %). Chloroform was removed by rotary evaporation, and the polymer was dried for 24 h at 65 °C in a vacuum oven. GPC was used to determine the molecular weight of PI. An amount of KCl was added that was 5 times the number of moles of PI chains. The sample was dried for 2 more days at 65 °C in a vacuum oven. Anhydrous THF (distilled first from potassium and then *n*-butyllithium) was added to the PI to dissolve it. The solution was titrated with potassium napthalide (∼1.0 M in THF) until a green color persisted. Ethylene oxide was then added to the PI solution, and the PEO was allowed to polymerize for 5 days. Polymerization was terminated with methanolic HCl. Solvent was removed by rotary evaporation, and the polymer was washed three times with water in chloroform (50/50 vol %). Chloroform was removed by rotary evaporation, and the polymer was placed in a vacuum oven for 3 days at 65 °C to remove naphthalene and residual water.

PI-b-PDMAEMA. sec-Butyllithium was used to initiate isoprene in cyclohexane. After 8 h of polymerization at room temperature, cyclohexane was removed on a vacuum line and anhydrous THF was subsequently added to the PI in a glovebox. A small amount of the PI was removed via syringe, terminated with methanolic HCl, and subjected to GPC to determine the PI MW. Polyisoprene was end-capped with a 5-fold excess of diphenylethylene and stirred for 30 min. The polymer solution was cooled to −60 °C before the addition of DMAEMA. Polymerization was allowed to proceed for several hours before the reaction was terminated with methanolic HCl. To purify the polymer, it was precipitated in cold methanol and dried on a vacuum line for several days.

The polymers were characterized by GPC to give the final polydispersity. ^{1}H NMR was used to determine the chemical composition of the block copolymer. The resulting polymers had number-average molecular weights in the range of 22−107 kg mol^{-1}, 67−90 wt % PI, and a polydispersity below 1.2; see Table 1.

Hybrid Preparation. Synthesis of mesostructured hybrids was performed by a one-pot synthesis approach, in which the ceramic precursor is expected to swell the hydrophilic block. Films were cast beneath a hemispherical dish made from the bottom half of a 1 L flask. Heating was controlled using a IKA RET control visc IKAMAG digital hot plate. The chemical structures of the block copolymers and the PUMVS are shown in Figure 1. In a typical synthesis a 5 wt % block copolymer solution in THF or toluene was mixed with the ceramic precursor and the radical initiator dicumyl peroxide (1 wt % with respect to the mass of PUMVS) and stirred for 1 h. The solution was subsequently poured into a Teflon Petri dish and a film cast by solvent evaporation on a hot plate at 50 °C followed by annealing for 24 h under vacuum at 50 °C. This resulted in a film thickness of about 500 μm. The temperature was then increased to 130 °C for 3 h to cross-link the PUMVS.

Results and Discussion

1. Morphology Diagram for PI-*b*-PDMAEMA/PUMVS Hybrids. The presence of a semicrystalline block in a block copolymer adds an extra level of complexity to the morphological behavior as microphase separation can be driven by both block incompatibility and crystallization. In order to better understand the morphological differences resulting from using a semicrystalline block copolymer as a structure directing agent for PDC precursors, it is insightful to compare the morphological behavior with hybrids from an amorphous block copolymer. To this end we used five different PI-*b*-PDMAEMA block copolymers with different PDMAEMA weight fractions (poly-

Scheme 1. Synthesis of PI-*b*-PEO and PI-*b*-PDMAEMA

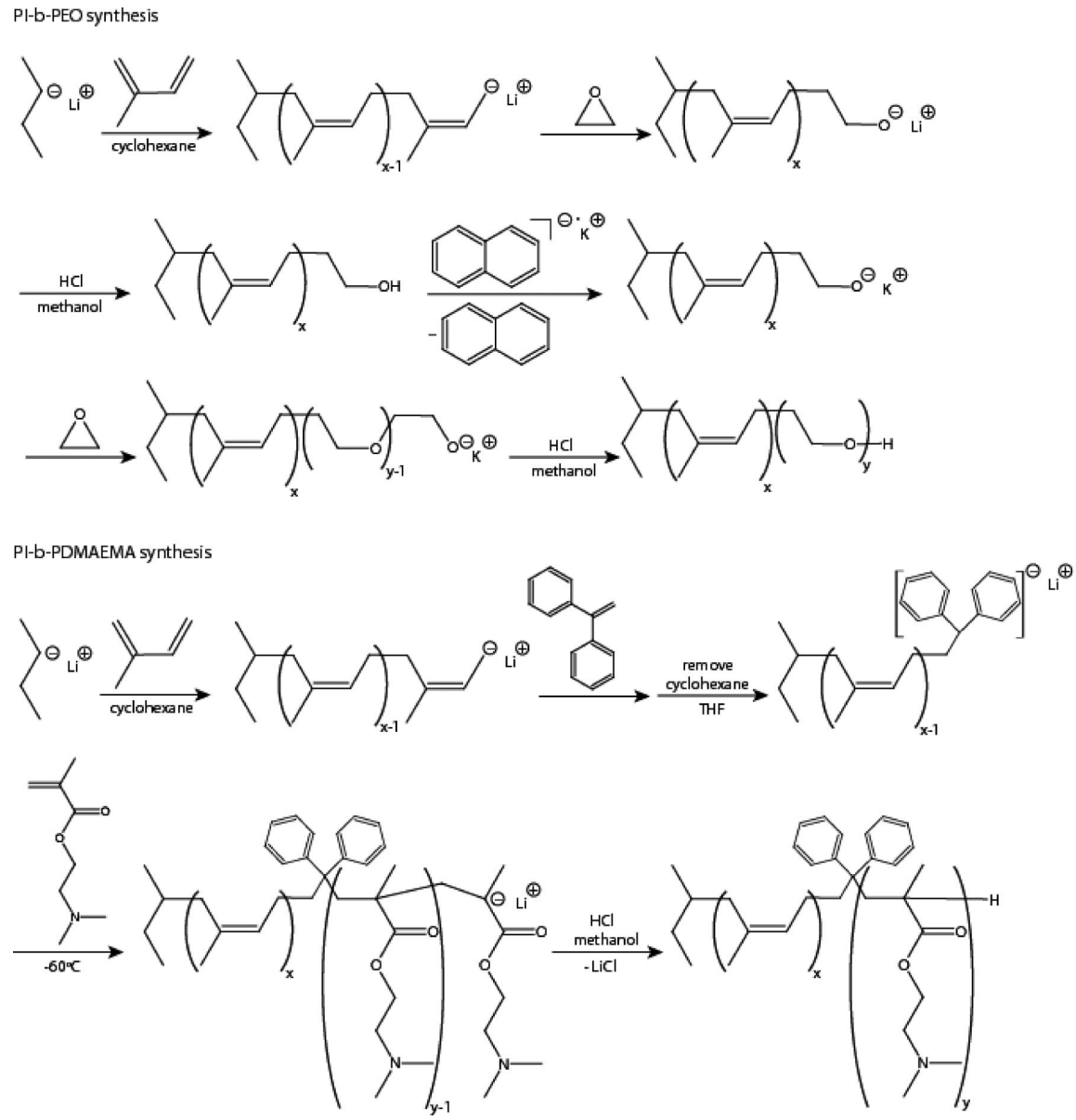

Table 1. Characterization of Block Copolymers

	block copolymer	MW (g/mol)	polydispersity	wt % PI
A	PI-*b*-PDMAEMA	107 200	1.03	90
B	PI-*b*-PDMAEMA	24 300	1.06	85
C	PI-*b*-PDMAEMA	29 000	1.04	83
D	PI-*b*-PDMAEMA	84 000	1.07	79
E	PI-*b*-PDMAEMA	31 100	1.05	67
F	PI-*b*-PEO	22 100	1.05	85

mers A−E in Table 1) and cast 25 films with PUMVS/block copolymer weight ratios ranging between 0.12 and 4.03 (see Experimental Section and Table 2). The resulting hybrid morphologies were determined by a combination of SAXS and TEM as described in refs 8 and 18 (see also below). The behavior of the PI-*b*-PDMAEMA/PUMVS system is depicted in the form of a morphology diagram in Figure 2, and results are summarized in Table 2.

The morphology map is based on the weight fraction of each component (PI, PDMAEMA, and PUMVS). In this diagram, from left to right, the five dark lines connect compositions derived from the five block copolymers by adding increasing amounts of the PDC precursor. Compositions showing the same hybrid morphology have been color-coded. We found lamellar (L), hexagonally packed cylinder (C), and body-centered cubic packed spherical (S) hybrid morphologies. The map demonstrates that by systematically increasing the PUMVS/block copolymer ratio multiple morphologies can be obtained from the same block copolymer. This is consistent with earlier TEM and SAXS studies on this system.[18] The white areas in Figure 2 provide a rough guide which part of phase space the different morphologies cover.

2. Comparison of PI-*b*-PDMAEMA/PUMVS with PI-*b*-PEO/PUMVS Hybrids. After exploring the PI-*b*-PDMAEMA/PUMVS hybrid morphology space, we subsequently compared the morphological behavior of two sets of hybrid samples: one derived from PI-*b*-PEO (polymer F in Table 1) and one from PI-*b*-PDMAEMA (polymer B in Table 1), i.e., from block copolymers with similar polymer characteristics. The polymers exhibited a hexagonally packed cylindrical morphology and *d*-spacings of 20.2 and 18.1 nm for PI-*b*-PEO and PI-*b*-PDMAEMA, respectively. Both sets of hybrids were prepared with very similar PUMVS/block copolymer weight ratios and under identical conditions (see Table 3 and Experimental

Table 2. Compositions of PI-*b*-PDMAEMA/PUMVS Hybrids

composite	PUMVS/PI-*b*-PDMAEMA weight ratio	morphology[a]	composite	PUMVS/PI-*b*-PDMAEMA weight ratio	morphology[a]
A-1	0.52	C	D-2	0.99	L
A-2	0.98	L	D-3	1.49	L
A-3	1.52	L	D-4	1.99	C
A-4	2.54	C	E-1	0.99	L
B-1	0.12	C	E-2	1.49	C
B-2	0.57	L	E-3	1.98	C
B-3	1.07	L	E-4	2.00	C
B-4	1.49	L	E-5	2.03	C
B-5	2.08	C	E-6	2.48	C
B-6	2.97	S	E-7	3.18	S
C-1	1.07	L	E-8	3.29	S
C-2	1.55	L	E-9	4.03	S
D-1	0.50	L			

[a] Cylindrical (C), lamellar (L), and spherical (S).

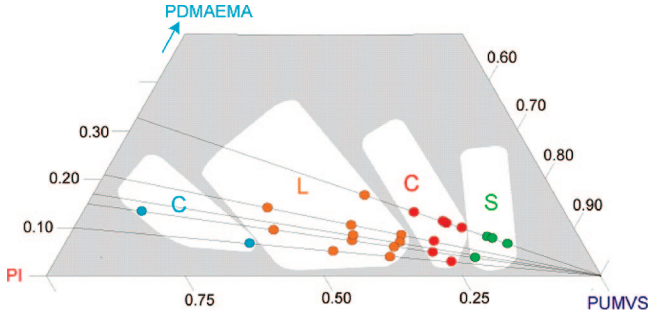

Figure 2. Morphology diagram mapping the morphologies for various weight fractions of the PI-*b*-PDMAEMA/PUMVS system. Compositions showing the same hybrid morphology are color-coded, and white domains suggest regions with well-defined hybrid morphologies: cylindrical (C) blue, lamellar (L) orange, cylindrical (C) red, and spherical (S) green. Dark lines connect compositions derived from a specific block copolymer by adding increasing amounts of PDC precursor.

Section). All of the cured samples were transparent, suggesting the lack of macroscopic phase separation between cross-linked PUMVS and block copolymer. TEM data corroborated this observation (see below). Macroscopic segregation may be prevented by mobility restrictions upon cross-linking and high free energy barriers to nucleation of block copolymer rich domains.[5] For the PI-*b*-PEO/PUMVS hybrids it is also very likely that the PUMVS is covalently bonded to the terminal hydroxy group of the PEO chain. Hydroxyl groups are known to react with PUMVS,[9,10,18] creating a PUMVS network attached to the PEO chains, thereby preventing macroscopic segregation.

2.1. Hybrid Morphology. Hybrid structure was investigated by a combination of SAXS and TEM. Figure 3 shows, side by side, stack plots of SAXS traces of the different hybrids with compositions described in Table 3. Comparing scattering traces suggests that structure evolution as a function of weight % PUMVS is very different for the two hybrid systems. SAXS traces of all but one of the PI-*b*-PEO/PUMVS hybrids (Figure 3a) show at least one higher order reflection at angular position of $\sqrt{4}$ of the first-order maximum, consistent with a lamellar morphology. Only PI-*b*-PEO/PUMVS hybrid 1 with only 11 wt % PUMVS shows a higher order reflection at angular position $\sqrt{3}$ of the first-order maximum, consistent with cylinders packed in a hexagonal lattice. In contrast, SAXS traces of PI-*b*-PDMAEMA/PUMVS hybrids 6 and 9 (Figure 3b) both show a (broad) higher-order peak around angular positions of $\sqrt{3}$ and $\sqrt{4}$ of the first-order maximum, consistent with cylinders packed in a hexagonal lattice. Hybrids 7 and 8 show at least one higher-order reflection at angular position of $\sqrt{4}$ and $\sqrt{9}$ of the first-order maximum, respectively, both consistent with a lamellar morphology. Finally, sample 10 shows a (broad) higher-order reflection around angular positions of $\sqrt{2}$ and $\sqrt{3}$ of the first-order maximum, consistent with a body-centered cubic packed spherical morphology. Thus, whereas the PI-*b*-PDMAEMA/PUMVS hybrid system shows a sequence of four morphologies upon increase of PUMVS content expected from e.g. mean-field calculations of block copolymers,[19,20] the structure evolution of the PI-*b*-PEO/PUMVS systems seems to get stuck once the lamellar morphology is reached.

The latter behavior is similar to that of pure PI-*b*-PEO, where independent of composition at low temperatures (below ~50 °C), upon PEO crystallization, phases revert to the crystalline lamellar morphology.[21] PI-*b*-PEO is an example of a strongly segregated system with soft confinement, with $T_{ODT} < T_c < T_g$, where T_{ODT} is the order−disorder transition (ODT) temperature, T_c is the crystallization temperature of the crystallizable block, and T_g is the glass-transition temperature of the amorphous block. The segregation strength between PI and PEO is sufficiently strong at molecular weights studied here to confine crystallization within spherical, cylindrical, or lamellar domains. Therefore, PI-*b*-PEO with a PEO weight fraction between 0.17 and 0.30 will form a hexagonally packed cylindrical morphology with the PEO crystals confined in cylinders, whereas polymers with PEO weight fractions larger than ~0.30 will all form the crystalline lamellar morphology. The SAXS data of the PI-*b*-

Table 3. Characterization of PI-*b*-PEO/PUMVS and PI-*b*-PDMAEMA/PUMVS Hybrids

sample	block copolymer	PUMVS/block copolymer weight ratio	*d*-spacing (nm)	*d*-spacing increase (%)	morphology
1	PI-*b*-PEO	0.12	24.6		C
2	PI-*b*-PEO	0.55	26.2	6.9	L
3	PI-*b*-PEO	1.05	27.3	10.6	L
4	PI-*b*-PEO	1.96	27.9	13.4	L
5	PI-*b*-PEO	2.50	29.7	20.7	L
6	PI-*b*-PDMAEMA	0.12	21.1		C
7	PI-*b*-PDMAEMA	0.57	23.4	10.9	L
8	PI-*b*-PDMAEMA	1.07	24.1	14.2	L
9	PI-*b*-PDMAEMA	2.08	27.7	31.3	C
10	PI-*b*-PDMAEMA	2.97	34.3	62.6	S
11	PI-*b*-PEO	2.30	29.6		L

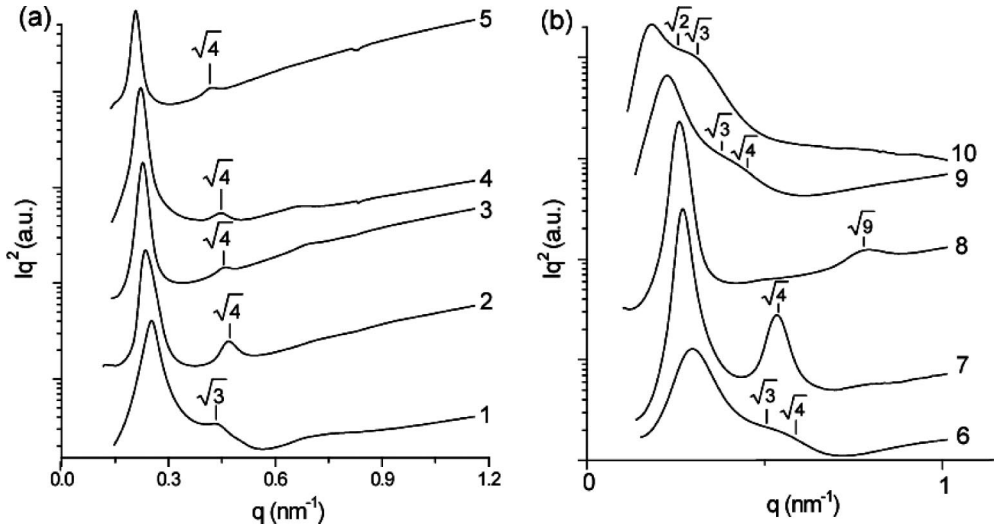

Figure 3. (a) SAXS traces of composite morphologies obtained by adding different amounts of PUMVS to same PI-*b*-PEO polymer (polymer F in Table 1). Data are consistent with (1) hexagonal cylinder morphology and (2−5) lamellar morphology. (b) SAXS traces of composite morphologies obtained by adding different amounts of PUMVS to the same PI-*b*-PDMAEMA polymer (polymer B in Table 1). Data are consistent with (6) hexagonal cylinder morphology, (7, 8) lamellar morphology, (9) hexagonal cylinder morphology, and (10) spherical morphology.

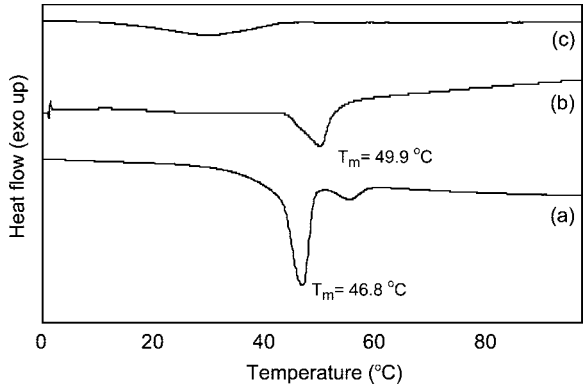

Figure 4. DSC heating curves (5 °C/min) of (a) PI-*b*-PEO block copolymer, (b) as-synthesized PI-*b*-PEO/PUMVS hybrid 2, and (c) PI-*b*-PEO/PUMVS hybrid 11 annealed at 300 °C.

PEO/PUMVS hybrids follow this trend, suggesting that PEO crystallizes even in the presence of cross-linked PUMVS. In order to support this hypothesis, we performed differential scanning calorimetry (DSC) measurements (see Figure 4).

Indeed, DSC curves of the pure PI-*b*-PEO block copolymer (Figure 4a) and of the PI-*b*-PEO/PUMVS hybrid 2 (Figure 4b) both show an endothermic peak upon heating associated with the melting of crystalline PEO. The double melting peak of PEO in the pure polymer (Figure 4a) is probably due to recrystallization during heating.[22,23]

2.2. Lattice Spacing. Further inspection of the two series of SAXS traces in Figure 3 reveals a difference in the relative shifts of first-order maxima and corresponding *d*-spacings upon addition of PUMVS. Whereas the first-order maxima of the PI-*b*-PDMAEMA/PUMVS system significantly moves to smaller *q* values upon increasing PUMVS content, those of the PI-*b*-PEO/PUMVS system only decrease slightly. Table 3 summarizes this result in the form of the respective lattice *d*-spacings. In order to rationalize this behavior, one has to separate the influence of the PUMVS on the PI and PEO domains. To this end, TEM was performed on lamellar hybrids 2−4 to determine the thickness ratio of the PI and PEO/PUMVS domains. Representative bright-field TEM images of PI-*b*-PEO/PUMVS hybrids 2, 3, and 4 are depicted in parts a, b, and c of Figure 5, respectively. The images show alternating layers of light (PI) and dark (PEO/PUMVS) lamellar domains, the

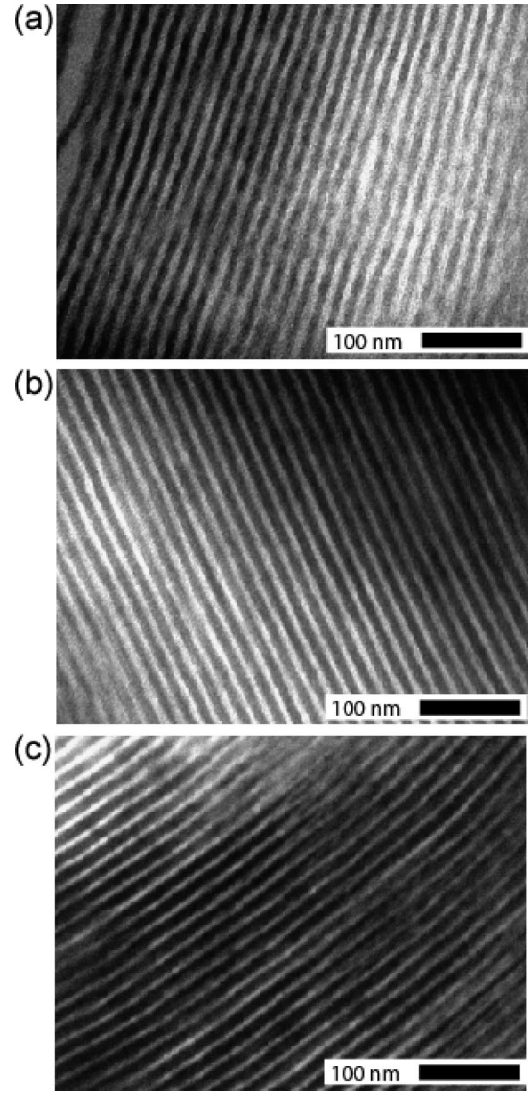

Figure 5. Bright-field TEM images revealing a lamellar morphology for hybrids 2 (a), 3 (b), and 4 (c).

contrast arising from the electron density difference between the domains. Closer inspection of these images reveals that with

Table 4. Comparison of Axial and Lateral Changes in the PEO/PUMVS Layer

sample	PUMVS/block copolymer weight ratio	PI layer thickness[a] (nm)	PEO/PUMVS layer thickness[a] (nm)	increase in axial direction (%)	area per junction[a] (nm^2)	increase in lateral direction (%)
2	0.55	15.7	10.5		5.14	
3	1.05	12.7	14.6	38.5	6.36	11.2
4	1.96	9.2	18.7	77.5	8.72	30.3
5	2.50	8.4	21.3	102	9.59	36.6

[a] Determined by SAXS.

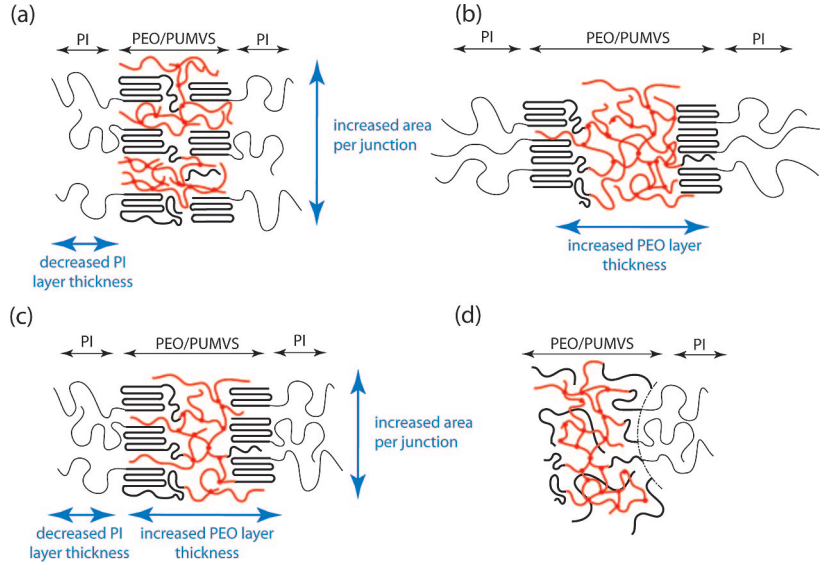

Figure 6. Schematic illustrating (a) lateral swelling, (b) axial swelling, (c) lamellar morphology in as-synthesized PI-*b*-PEO/PUMVS hybrid, and (d) cylindrical morphology for annealed PI-*b*-PEO/PUMVS.

increasing PUMVS content the thickness of the PI domains decreases while that of the PEO/PUMVS domains increases. This is corroborated by a more quantitative analysis of the SAXS data of Figure 3.

The individual layer thicknesses can be calculated from these SAXS data using

$$l_{\mathrm{PEO/PUMVS}} = \Phi_{\mathrm{PEO/PUMVS}} L \tag{1}$$

$$l_{\mathrm{PI}} = L - l_{\mathrm{PEO/PUMVS}} = (1 - \Phi_{\mathrm{PEO/PUMVS}}) L \tag{2}$$

where $\Phi_{\mathrm{PEO/PUMVS}}$ is the effective PEO/PUMVS volume fraction and L the d-spacing provided by SAXS. The effective volume fractions are calculated based on the original volume fractions of the PI-*b*-PEO block copolymer, the PUMVS/block copolymer ratio, and the densities of PI, PEO, and PUMVS (0.91, 1.12, and 1.12 g/cm^3), respectively.[24,25] Results are given in Table 4. The increase in axial direction tabulated in Table 4 is the increase in PEO/PUMVS layer thickness of hybrids 3−5 compared to hybrid 2. The increase is not compared to pure PI-*b*-PEO block copolymer or hybrid 1 as they exhibit a cylindrical and not a lamellar structure.

The TEM images and SAXS data analysis both show that with increasing PUMVS loading the PEO/PUMVS layer thickness increases while the PI layer thickness decreases. The decrease in PI layer thickness can be related to the large degree of stretching induced in the PI block upon crystallization of the PEO block. Because the two blocks are covalently bound together and the constraint of constant density, if the PEO layer thickens upon crystallization, the amorphous PI chains must stretch to thicken the PI layer proportionally. The highly stretched conformation of the PI chains provides a driving force for the solubilization of PUMVS in the PEO block as the PI chains are allowed to relax to a more random coil conformation. The addition of PUMVS to the PEO block thus reduces the conformational free energy of the PI block and leads to a decrease in PI layer thickness.

The increase in PEO/PUMVS layer thickness with increasing PUMVS loading is due to the preferential swelling of the PEO chains with the PUMVS. The possibility of complete segregation of PUMVS in the middle of the PEO domain, and thereby simply increasing the volume, is excluded because this kind of distribution does not lead to conformational changes in the block copolymer; i.e., no change in PI layer thickness would have been observed. However, the PUMVS does not necessarily swell the PEO chains throughout the PEO/PUMVS domain to the same extent; i.e., the PUMVS does not have to be uniformly distributed throughout the PEO/PUMVS layer. To investigate the symmetry of the swelling, the average interfacial area per copolymer junction of the PI-*b*-PEO interface is calculated from SAXS data (assuming that the PUMVS does not penetrate the PI block and that the interface between the PI and PEO domains is narrow). The average area per chain junction for a lamellar morphology is given by[26]

$$\sigma_j = \frac{2M_{\mathrm{PI}}}{N_{\mathrm{Av}} \rho_{\mathrm{PI}} (1 - \Phi_{\mathrm{PEO/PUMVS}}) L} \tag{3}$$

where M_{PI} is the number-average molecular weight of the PI block, N_{Av} is Avogadro's number, and ρ_{PI} is the PI density. Whereas the individual layer thicknesses, calculated above, are a measure of the axial changes perpendicular to the PI-*b*-PEO interface, the area per junction is a measure of the lateral changes parallel to the PI-*b*-PEO interface. Figure 6a,b schematically illustrates lateral swelling versus axial swelling in the PI-*b*-PEO/PUMVS hybrids, and results of the calculations are summarized in Table 4.

From Table 4, the area per junction increases upon increasing amount of PUMVS. Comparing the increase of the PEO/PUMVS layer thickness to the increase in area per junction of

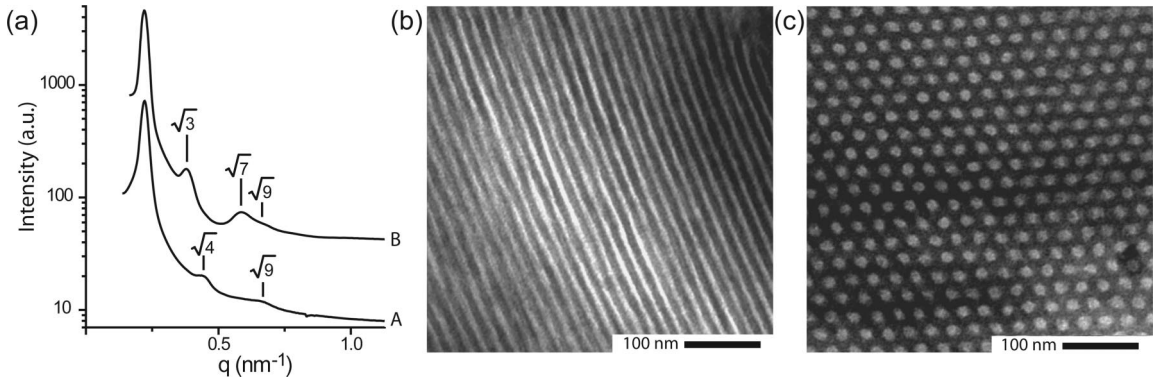

Figure 7. Morphology of PI-*b*-PEO/PUMVS hybrids subjected to different heat treatments. (a) SAXS traces for hybrid 11: A, as-synthesized; B, annealed at 300 °C. Bright-field TEM images of hybrid 11. (b) As-synthesized. (c) Annealed at 300 °C.

a hybrid gives an indication of the symmetry of the swelling. As was previously shown for blends of poly(isoprene-*block*-styrene) (PI-*b*-PS) diblock copolymers with polystyrene homopolymers,[26−28] PS homopolymer (with molecular weights comparable to the PS block in the block copolymer) preferentially mixes with the PS block segments away from the PS-*b*-PI interface to prevent a loss in entropy for the homopolymer due to spatial constraints. In this PI-*b*-PS/PS system, upon increased loading of PS homopolymers, a lower bound plateau for the PI layer thickness and a limit for the lateral swelling were observed. In the present system the swelling of the lamellar PEO domains is also larger in the axial direction than in the lateral direction, indicating a nonuniform distribution of PUMVS within the lamellae, with the highest PUMVS segment density at the center of the lamellae. The changes in the present system are schematically represented in Figure 6c. However, no lower limit for the PI layer thickness or limit in lateral swelling is observed, even though both the molecular weight and the loading of the cross-linked PUMVS are much higher than that of the PS homopolymers in the earlier study.

The increased lateral swelling as compared to the PI-*b*-PS/PS system is caused by relaxation of the highly stretched PI chains, as described above. Therefore, the tendency for PUMVS localization at the domain centers is smaller for the present system compared to the PI-*b*-PS/PS system. The good structural regularity in the hybrids observed in TEM even upon high PUMVS loadings also indicates this. A high degree of lateral swelling was also found for blends of semicrystalline polyethylene−poly(ethylene-*alt*-propylene) diblock copolymers with semicrystalline polyethylene homopolymers.[29] This was explained by relief of chain stretching of the amorphous block as well. Thus, our data suggest that upon PUMVS loading the PI chain stretching relaxes by swelling the PEO domains in the lateral direction, resulting in a smaller increase in the overall structural periodicity in the PI-*b*-PEO/PUMVS system relative to the amorphous PI-*b*-PDMAEMA/PUMVS system.

2.3. Order−Order Phase Transitions. It was previously shown for a polybutadiene-*block*-poly(ethylene oxide) diblock copolymer/PUMVS system[9,10] that upon annealing at elevated temperatures the system could undergo order−order phase transitions, leading to morphologies in the structural evolution beyond lamellar. As this system is very similar to the present system, annealing was explored in order to try out the same thing for the PI-*b*-PEO/PUMVS system. To this end, a hybrid with a PUMVS/PI-*b*-PEO ratio of 2.3 (hybrid 11) was annealed at 300 °C for 5 h. The morphology of this annealed hybrid was investigated with SAXS and TEM and results compared to the as-synthesized material.

Figure 7a shows the respective SAXS traces. As-synthesized hybrid 11 shows higher-order reflections at angular positions of $\sqrt{4}$ and $\sqrt{9}$ of the first-order maximum, consistent with a lamellar morphology. This is corroborated by TEM (Figure 7b) and is consistent with the results discussed earlier; see Table 3 (compare samples 3, 4, and 11). The SAXS trace of the same sample after annealing at 300 °C shows higher-order reflections at angular positions of $\sqrt{3}$, $\sqrt{7}$, and $\sqrt{9}$ of the first-order maximum, consistent with cylinders packed in a hexagonal lattice. The TEM image in Figure 7c clearly shows the hexagonal packing of light (PI) cylinders in a dark (PDMAEMA/PUMVS) matrix. The TEM observations thus corroborate the interpretation of the SAXS data.

The effective PEO/PUMVS volume fraction of this hybrid is 0.70. Pure PI-*b*-PEO with a similar composition shows the same type of order−order phase transition upon heating.[21] But in case of the PI-*b*-PEO/PUMVS hybrid the system is prevented from going back to the crystalline lamellar morphology upon cooling to temperatures below the PEO crystallization temperature; see also Figure 6d. The DSC curve of hybrid 11 in Figure 4c does not show a melting peak, corroborating this hypothesis. This change in behavior is not due to polymer degradation. We cross-checked that pure PI-*b*-PEO after the same heat treatment still shows a strong melting peak in DSC. Rather, heating to higher temperatures first leads to PEO crystal melting and better mixing of PEO chains with the PUMVS. Upon further annealing at elevated temperatures the mobility of the PEO chains is expected to be diminished due to increased covalent coupling of the PEO chains to the PUMVS discussed earlier and to progressing cross-linking between the PUMVS molecules,[30] adding barriers to crystallization.

Order−order phase transitions were also found in block copolymer epoxy−resin mixtures.[5] These transitions were caused by the local segregation of PEO out of the epoxy matrix. This results in a smaller effective PEO/epoxy volume fraction, and therefore morphologies with flatter interfaces become more stable. The order−order phase transition observed in the present system is not a transition toward a flatter interface and therefore cannot be explained by segregation of PEO out of the PUMVS matrix. The covalent bonding between the terminal hydroxy group of the PEO chain and the PUMVS is thought to prevent complete segregation between the PEO and the PUMVS.

Conclusions

The effect of using a semicrystalline diblock copolymer, PI-*b*-PEO, versus an amorphous block copolymer, PI-*b*-PDMAEMA, as structure directing agent for a polymer derived ceramic precursor, PUMVS, on hybrid morphology was investigated. The PUMVS preferentially swells the hydrophilic block of both block copolymers, and by systematically increasing the PUMVS/block copolymer ratio a sequence of (up to four)

morphologies were obtained from a single amorphous PI-*b*-PDMAEMA block copolymer, which is expected from typical block copolymer phase diagrams. However, in the case of PI-*b*-PEO a crystalline lamellar morphology is obtained for most PUMVS/block copolymer ratios, upon crystallization of the PEO. The overall periodicity of the PI-*b*-PEO/PUMVS hybrids increased only slightly upon PUMVS loading because the strong chain stretching in the PI block is progressively relaxed as the PUMVS swells the PEO. Suppression of the crystallization through high-temperature annealing results in morphological behavior similar to the amorphous PI-*b*-PDMAEMA/PUMVS system.

Acknowledgment. The authors thank Arthur Woll for help with the SAXS experiments and Lewis Fetters for discussions. The financial support of the National Science Foundation (Award DMR-0605856) is gratefully acknowledged. The work was further supported by the Cornell Center for Materials Research (CCMR), a Materials Research Science and Engineering Center of the National Science Foundation (DMR-0520404). CHESS is supported by the NSF & NIH/NIGMS via NSF Award DMR-0225180.

References and Notes

(1) Templin, M.; Franck, A.; DuChesne, A.; Leist, H.; Zhang, Y. M.; Ulrich, R.; Schadler, V.; Wiesner, U. *Science* **1997**, *278*, 1795–1798.
(2) Yang, P.; Zhao, D.; Margolese, D. I.; Chmelka, B. F.; Stucky, G. D. *Nature (London)* **1998**, *396*, 152–155.
(3) Wan, Y.; Zhao, D. Y. *Chem. Rev.* **2007**, *107*, 2821–2860.
(4) Hillmyer, M. A.; Lipic, P. M.; Hajduk, D. A.; Almdal, K.; Bates, F. S. *J. Am. Chem. Soc.* **1997**, *119*, 2749–2750.
(5) Lipic, P. M.; Bates, F. S.; Hillmyer, M. A. *J. Am. Chem. Soc.* **1998**, *120*, 8963–8970.
(6) Kosonen, H.; Ruokolainen, J.; Nyholm, P.; Ikkala, O. *Macromolecules* **2001**, *34*, 3046–3049.
(7) Garcia, C. B. W.; Lovell, C.; Curry, C.; Faught, M.; Zhang, Y. M.; Wiesner, U. *J. Polym. Sci., Part B: Polym. Phys.* **2003**, *41*, 3346–3350.
(8) Kamperman, M.; Garcia, C. B. W.; Du, P.; Ow, H. S.; Wiesner, U. *J. Am. Chem. Soc.* **2004**, *126*, 14708–14709.
(9) Wan, J. L.; Alizadeh, A.; Taylor, S. T.; Malenfant, P. R. L.; Manoharan, M.; Loureiro, S. M. *Chem. Mater.* **2005**, *17*, 5613–5617.
(10) Wan, J.; Malenfant, P. R. L.; Taylor, S. T.; Loureiro, S. M.; Manoharan, M. *Mater. Sci. Eng., A* **2007**, *463*, 78–88.
(11) Malenfant, P. R. L.; Wan, J.; Taylor, S. T.; Manoharan, M. *Nat. Nanotechnol.* **2007**, *2*, 43–46.
(12) Nghiem, Q. D.; Kim, D. J.; Kim, D. P. *Adv. Mater.* **2007**, *19*, 2351–2354.
(13) Nghiem, Q. D.; Kim, D. P. *Chem. Mater.* **2008**, *20*, 3735–3739.
(14) Freer, E. M.; Krupp, L. E.; Hinsberg, W. D.; Rice, P. M.; Hedrick, J. L.; Cha, J. N.; Miller, R. D.; Kim, H. C. *Nano Lett.* **2005**, *5*, 2014–2018.
(15) Allgaier, J.; Poppe, A.; Willner, L.; Richter, D. *Macromolecules* **1997**, *30*, 1582–1586.
(16) Renker, S. Doctoral Dissertation, Max Planck Institute for Polymer Research, Mainz, Germany, 2003.
(17) Creutz, S.; Teyssie, P.; Jerome, R. *Macromolecules* **1997**, *30*, 6–9.
(18) Kamperman, M.; Du, P.; Scarlat, R. O.; Herz, E.; Werner-Zwanziger, U.; Graf, R.; Zwanziger, J. W.; Spiess, H. W.; Wiesner, U. *Macromol. Chem. Phys.* **2007**, *208*, 2096–2108.
(19) Matsen, M. W.; Bates, F. S. *Macromolecules* **1996**, *29*, 7641–7644.
(20) Khandpur, A. K.; Forster, S.; Bates, F. S.; Hamley, I. W.; Ryan, A. J.; Bras, W.; Almdal, K.; Mortensen, K. *Macromolecules* **1995**, *28*, 8796–8806.
(21) Floudas, G.; Vazaiou, B.; Schipper, F.; Ulrich, R.; Wiesner, U.; Iatrou, H.; Hadjichristidis, N. *Macromolecules* **2001**, *34*, 2947–2957.
(22) Holdsworth, P. J.; Turner-Jones, A. *Polymer* **1971**, *12*, 195–208.
(23) Lemstra, P. J.; Challa, G.; Kooistra, T. *J. Polym. Sci., Polym. Phys. Ed.* **1972**, *10*, 823–833.
(24) Brandrop, J.; Immergut, E. H. *Polymer Handbook*; Wiley: New York, 1975.
(25) CERASET SN Inorganic Polymer Technical Bulletin, Lanxide Co., 1997.
(26) Winey, K. I.; Thomas, E. L.; Fetters, L. J. *Macromolecules* **1991**, *24*, 6182–6188.
(27) Hashimoto, T.; Tanaka, H.; Hasegawa, H. *Macromolecules* **1990**, *23*, 4378–4386.
(28) Tanaka, H.; Hasegawa, H.; Hashimoto, T. *Macromolecules* **1991**, *24*, 240–251.
(29) Rangarajan, P.; Haisch, C. F.; Register, R. A.; Adamson, D. H.; Fetters, L. J. *Macromolecules* **1997**, *30*, 494–502.
(30) Li, Y. L.; Kroke, E.; Riedel, R.; Fasel, C.; Gervais, C.; Babonneau, F. *Appl. Organomet. Chem.* **2001**, *15*, 820–832.

MA801458W